Phase behaviour of model fluids interacting through short-range forces

2002 J. Phys.: Condens. Matter 14 2181

(http://iopscience.iop.org/0953-8984/14/9/307)

INSTITUTE OF PHYSICS PUBLISHING JOURNAL OF PHYSICS: CONDENSED MATTER

J. Phys.: Condens. Matter **14** (2002) 2181–2191 PII: S0953-8984(02)31173-1

Phase behaviour of model fluids interacting through short-range forces

D Costa, C Caccamo[1] and M C Abramo

Istituto Nazionale per la Fisica della Materia (INFM) and Dipartimento di Fisica, Università di Messina, Contrada Papardo, CP 50, 98166 Messina, Italy

E-mail: caccamo@tritone.unime.it

Received 22 November 2001
Published 22 February 2002
Online at stacks.iop.org/JPhysCM/14/2181

Abstract

Computer simulation investigations of two model fluids interacting through short-range forces are presented. In one case, the chosen potential parameters make the model suitable to represent C_{60} fullerenes. For such a system, Monte Carlo calculations of the free energy are performed in order to determine the solid–liquid coexistence line and the whole phase diagram. In the other case, the potential is adapted to model the interaction between globular proteins in aqueous solutions, by obtaining a system whose phase diagram is known to have only metastable liquid–vapour equilibrium. We report on a previous study of such a fluid, concerning extensive molecular dynamics simulations of the crystallization process, and discuss the related results in the present context. The peculiar features of the phase behaviour of the two model systems, as well as their sensitive dependence on the potential properties, are also documented.

1. Introduction

Model fluids interacting through short-range forces are of current interest in the study of a number of physical systems constituted by macroparticles; the basic reason for such attention is that systems such as, e.g. protein solutions [1] or colloidal suspensions [2], are to a first approximation representable as one-component fluids in which the macromolecules or the colloidal particles are assumed to interact via a pairwise 'effective' potential which takes into account in an averaged manner the presence of the solvent and of other diluted particle species. A similar modelization can also be adopted for C_{60} [3, 4] and C_{70} [5] fullerenes, and for metal dichalcogenides [6]; in these systems, in fact, the interaction among atoms belonging to different molecules can be integrated over the molecular surfaces to yield a much simpler sphericalized pair potential [3].

[1] Author to whom any correspondence should be addressed.

A main topic in the physics of such model one-component fluids is to establish the role of solid–liquid versus solid–vapour equilibrium in determining the phase portrait of the system; in particular, one is interested to ascertain whether the nature of the interaction forces is such to prevent the formation of a stable liquid phase. This point is of interest in order to predict the phase behaviour of colloidal suspensions, a knowledge crucially important in many industrial processes. Also, the possible existence of liquid carbon, in the fullerene molecular form, has obviously attracted great attention early on since this hypothesis has been supported by specific calculations [7]. Finally, the interplay of the solid–vapour versus the solid–liquid transition appears to be directly involved in the process of protein crystallization [8], a phenomenon which still remains substantially unpredictable inasmuch as it has usually been tackled on the basis of empirical experimental protocols [9]. In this same concern, one is also interested to test the capability of the adopted modelization in order to cope with the complex processes of nucleation and crystal growth observed in real protein solutions.

In this work we report the results of extensive computer simulation studies concerning the mentioned different issues. In particular, we investigate the phase behaviour of two different short-range model potentials suited to describe, under appropriate choices of the potential parameters, fullerene materials or protein solutions.

We first consider C_{60} fullerene. The existence of a stable liquid phase for such a system, modelled in terms of rigid sphericalized molecules by Girifalco [3], has been the object of initial controversy [7, 10]. We here determine by means of Monte Carlo (MC) simulations the free energy of the fluid and solid phase of the Girifalco model of C_{60}, and compare the phase diagram that we obtain with previous predictions [7, 11, 12]; we are thus able to assess both the presence of a liquid pocket in the phase diagram of the model, and the accuracy of one-phase freezing criteria [13, 14] in terms of which the boundaries of the liquid phase have elsewhere been established [7, 11, 15].

We then consider a generalized Lennard-Jones model, whose phase diagram mimics that of a typical globular protein solution [16], and report the main conclusions presented in two previous papers [17] concerning the kinetics of crystallization of such a system. In these works, very long molecular dynamics (MD) simulations were performed along a thermodynamic path which extends far beneath the sublimation line of the system, to reach the metastable liquid–vapour binodal; this allows one to monitor the onset of nucleation and the early formation of ordered solid aggregates. We discuss these results in the present more general context of the relationship between the model potential features and the associated phase behaviour.

It is worth noting that the connection established here between the model potentials and specific systems is by no means unique, and therefore the results are open to a more general applicability than reported here.

2. Free energy determination of the phase diagram of C_{60}

In substantial agreement with the early predictions of Cheng *et al* [7], recent theoretical and computer simulation investigations [11, 12, 15] of the Girifalco model of C_{60} [3] have confirmed that this system possesses a stable liquid phase, albeit this turns out to be confined to a relatively small temperature range, when compared with the magnitude of the estimated critical temperature [12]. This peculiar feature of the phase diagram is basically related to the characteristics of the intermolecular potential whose short-range nature makes C_{60} a borderline system for the existence of the liquid phase, as it will be further confirmed by the present study.

We recall that the Girifalco potential, displayed in figure 1, is written as

$$V(r) = -\alpha_1 \left[\frac{1}{s(s-1)^3} + \frac{1}{s(s+1)^3} - \frac{2}{s^4} \right] + \alpha_2 \left[\frac{1}{s(s-1)^9} + \frac{1}{s(s+1)^9} - \frac{2}{s^{10}} \right] \tag{1}$$

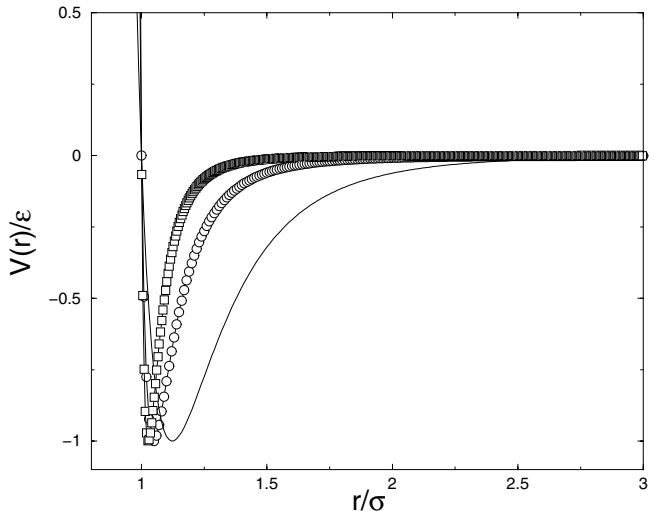

Figure 1. The C_{60} model potential of equation (1) (circles) and the generalized Lennard-Jones potential of equation (4) (squares); also displayed, the Lennard-Jones 12-6 potential (curve).

where $s = r/d, \alpha_1 = N^2A/12d^6$, and $\alpha_2 = N^2B/90d^{12}$; N and $d = 0.71$ nm are the number of carbon atoms and the diameter, respectively, of the fullerene particles, $A = 32 \times 10^{-60}$ erg cm^6 and $B = 55.77 \times 10^{-105}$ erg cm^{12} are constants entering the Lennard-Jones 12-6 potential through which two carbon sites on different sphericalized molecules are assumed to interact.

We display $V(r)$ in figure 1, by adopting reduced energy and length units, ϵ and σ, respectively, ϵ being the depth of the potential well and σ the (finite) distance at which $V(r)$ vanishes (i.e. $V(\sigma) = 0$). It is easy to recognize from the figure that as r increases beyond the deep minimum position, $V(r)$ approaches zero values within a distance approximately equal to 2σ, that is, with a much faster decay than the Lennard-Jones potential, also shown in figure 1.

The extension in temperature of the liquid phase is obviously given by the difference between the critical and the triple point temperatures; it thus becomes crucial, for the purpose of a confident estimate of such a range, to obtain an accurate determination of both the liquid–vapour binodal and the freezing line of the system.

As far as the determination of liquid–vapour equilibrium in C_{60} is concerned, extensive Gibbs ensemble MC simulations for the Girifalco model have been reported by two of us some time ago [11]; the related results were later substantially confirmed by free energy calculations based on MC simulations [12]. The knowledge of such an equilibrium line can then be considered as quite well assessed.

Turning now to the determination of the solid–liquid equilibrium in the same model, free energy calculations have also been reported in [12], resulting in a temperature range of existence of the liquid phase sensibly smaller than that reported in [7]. In [7], as well as in other related papers [11, 15], however, the freezing boundary was determined by using liquid state integral equation theories, supplemented by one-phase freezing criteria [13, 14]. These latter typically rest on peculiar values attained by some structural or thermodynamic quantity of the fluid phase, and the ensuing freezing line determinations are, of course, less rigorous than those based on the much more demanding free energy calculations. The emerging discrepancy between the two sets of results is certainly worthy of assessment; this is the first point, in fact, that we address in this work.

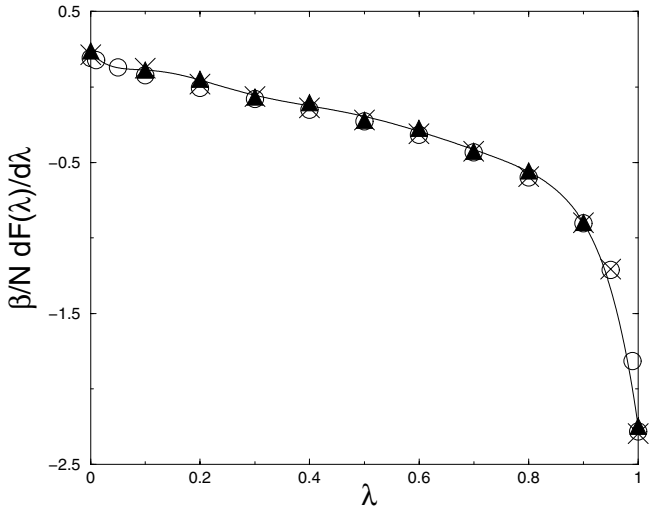

Figure 2. The integration path over λ which transforms the C_{60} solid (λ = 0) into an Einstein crystal (λ = 1, see text), at $T = 2100$ K and $\rho = 1.375\ \mathrm{nm}^{-3}$, and for several system sizes; circles, $N = 256$; triangles, $N = 864$; crosses, $N = 2916$. The curve is a smooth interpolation of the $N = 864$ data points.

Specifically, we report new and extensive MC estimates of the free energy in both the solid (fullerite) and the liquid phase of the Girifalco C_{60} model, subject to a careful control of the dependence of the results on the simulation conditions. These calculations, in conjunction with the previous Gibbs Ensemble determination of the liquid–vapour binodal [11], allow us to fully predict the phase diagram of the model.

First of all, the free energy F along the supercritical isotherm $T = 2100$ K has been determined as a function of the density ρ by integrating the equation of state along the fluid and the solid branch of the system [18]:

$$\frac{\beta F(\rho)}{N} - \frac{\beta F(\bar{\rho})}{N} = \int_{\bar{\rho}}^{\rho} \frac{\beta P(\rho')}{\rho'} \frac{\mathrm{d}\rho'}{\rho'}. \tag{2}$$

Here, $P(\rho)$ is the pressure of the system at a given density ρ and β is the inverse of the temperature in units of the Boltzmann constant k_B; $\bar{\rho}$ is a suitable reference density, for which the thermodynamic potentials are exactly known (see later). The equation of state of the system is then determined through standard MC simulations, at constant pressure or constant volume, on a sample composed of $N = 864$ particles enclosed in a cubic box with periodic boundary conditions.

As far as the reference free energy of the solid phase, $F_s(\bar{\rho})$, is concerned, this has been determined according to the well established Frenkel and Ladd [19] procedure, by performing a thermodynamic integration over a coupling parameter λ which transforms the C_{60} interaction in the solid fullerite into a corresponding harmonic coupling with the lattice sites (Einstein crystal) at the same density [20]; the results at $\bar{\rho} = 1.37\ \mathrm{nm}^{-3}$ are shown in figure 2. Then the integration over λ fully determines the C_{60} free energy $F_s(\bar{\rho} = 1.37)$. An investigation of the dependence of the free energy on the number of particles, performed with $N = 256$, 864 and 2916 particles, is also reported in figure 2; it appears that the size of the system has almost negligible effect on the behaviour of $F_s(\bar{\rho})$.

Turning now to the reference free energy of the liquid phase, $F_l(\bar{\rho})$ at $T = 2100$ K, this has been calculated at the intermediate density $\bar{\rho} = 0.6\ \mathrm{nm}^{-3}$, through the Widom test particle

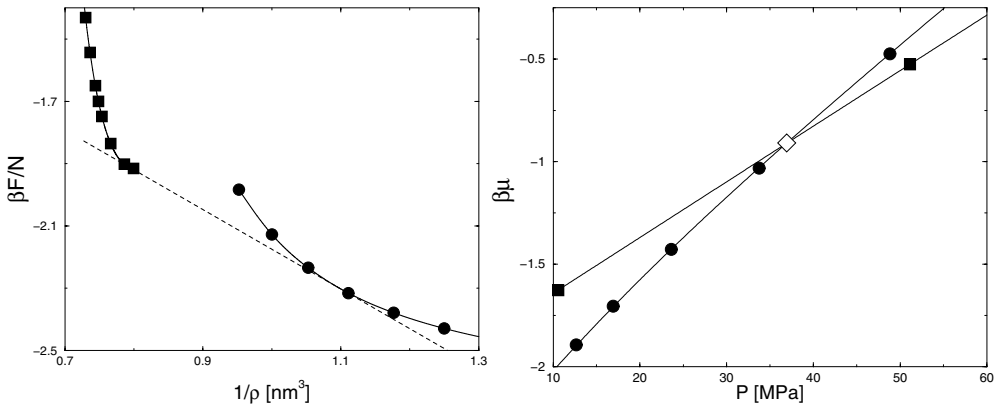

Figure 3. Free energy (left) and chemical potential (right) of the C_{60} model at $T = 2100$ K; squares: solid phase; circles: liquid phase; the full curves are smooth interpolations of the data points. The dashed line in the left panel is the common tangent to both branches; in the right panel, the diamond indicates the coexistence pressure.

method [20,21]. At this density, a stable statistics for the excess chemical potential of the fluid was cumulated over MC block runs of about $5 \times 30\,000$ steps, with a MC step consisting of a trial displacement of each particle, followed by as many as ∼50 trial insertions of a ghost particle in the sample.

The behaviour of the free energy, along the isotherm $T = 2100$ K, determined through (2), is displayed in the left panel of figure 3 as a function of the inverse of the density. The equilibrium condition follows by the equality of the chemical potential as a function of the pressure in both the liquid and the solid phase (figure 3, right panel); obviously, this condition corresponds to the common tangent construction also shown in the left panel of figure 3. The coexisting densities can then be obtained from the equilibrium pressure, through the equation of state P versus ρ, displayed in figure 4.

Once the thermodynamic potentials are known along the same isotherm, the free energy at different temperatures can be calculated by a straightforward integration of the internal energy U along an isochore path, according to the formula

$$\frac{\beta F(T)}{N} - \frac{\beta F(\bar{T})}{N} = -\int_{\bar{T}}^{T} \frac{U(T')}{N k_B T'} \frac{\mathrm{d}T'}{T'} \tag{3}$$

where $\bar{T} = 2100$ K. Four isochores in the liquid range $\rho = 0.80$–0.95 nm^{-3}, and three isochores in the solid phase at $\rho = 1.25$, 1.27 and 1.30 nm^{-3}, respectively, have been characterized in this way. The calculation of the coexisting densities follows the procedure outlined earlier, resulting in the phase diagram displayed in figure 5. We observe that the liquid branch of the chemical potential crosses the solid branch only for $T > 1850$ K; below this temperature, the intersection is shifted to the vapour side of the binodal, thus giving rise to a solid–vapour equilibrium, as shown in figure 5. The chemical potential of the vapour phase at $T = 1850$ K has been calculated by a direct Widom test in the density range $\rho = 0.1$–0.2 nm^{-3}.

The present investigation of the solid–liquid coexistence, combined with our previous Gibbs Ensemble calculation of the binodal line, also displayed in figure 5, yields a triple point temperature T_{tr} immediately above $T = 1850$ K, our freezing line resulting slightly shifted to higher density with respect to that reported in [12], where a $T_{tr} = 1880$ K estimate is given.

In figure 4 we also report the equilibrium liquid density that would be predicted by the one-phase entropic criterion of freezing [13] adopted in previous works. It appears that this approach

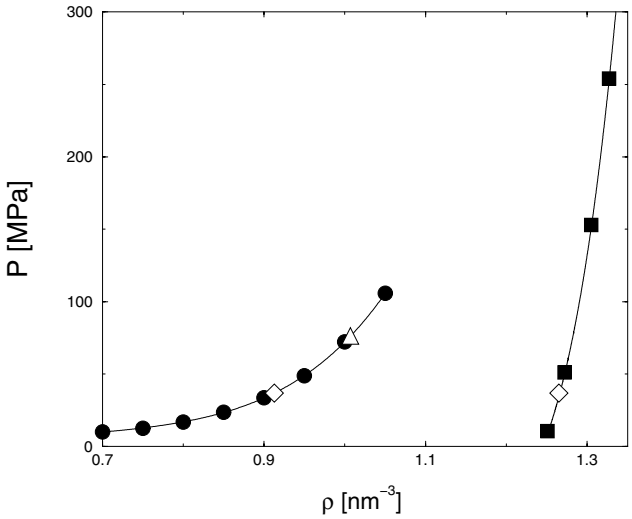

Figure 4. Equation of state of the C_{60} model at $T = 2100$ K. Squares: solid phase; circles: liquid phase; the full curves are smooth interpolations of the data points; the coexisting densities are shown as diamonds; the triangle indicates the estimate of the coexistence liquid density according to the one-phase entropic criterion.

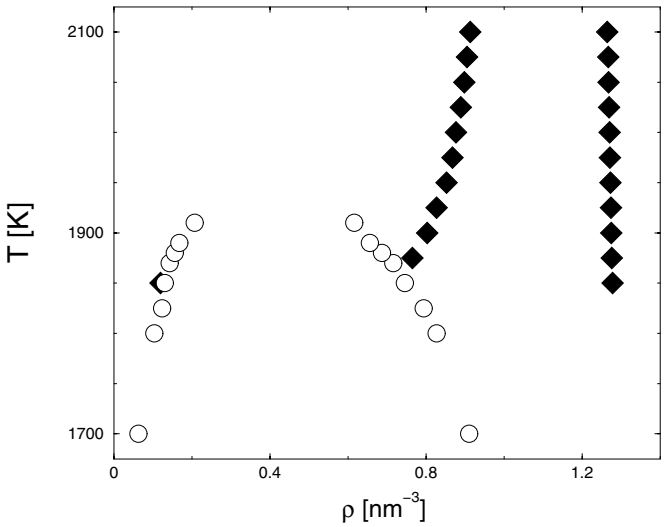

Figure 5. The phase diagram of the Girifalco C_{60} model. Diamonds: fluid–solid coexistence; circles: liquid–vapour binodal line, according to Gibbs Ensemble calculations of [11].

leads to an overestimate of the freezing density by approximately 10% at $T = 2100$ K. The related shift of the freezing line to higher densities results in a lower triple point temperature, which in fact has been estimated as low as ∼1500–1700 K, depending on the integral equation theory adopted [7, 11, 15].

We point out that the trend to overestimate the freezing density is not unique to the adopted entropic criterion, and that similar results are obtained [22] if the Hansen–Verlet prescription [14] for the height of the structure factor in the liquid phase is used. On the other

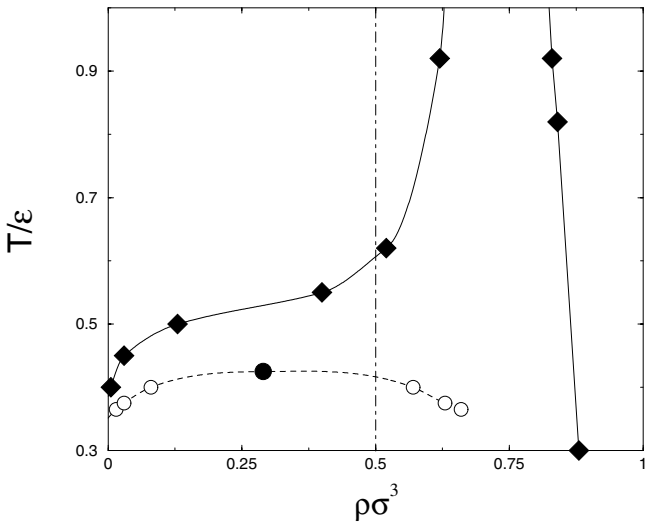

Figure 6. Phase diagram of the generalized Lennard-Jones potential of (4), displayed in figure 1. The dashed curve indicates the metastable liquid–vapour separation; simulations have been performed along the isochore path represented by the vertical dot-dashed line.

hand, these one-phase criteria are known to work quite accurately for hard sphere fluids, and for fluids characterized by very repulsive potentials at short range [23, 24]. It is interesting to recall in this concern that Louis [25] have recently proposed a classification of fluids in two broad categories, according to whether the physical behaviour of these systems is dominated by excluded volume effects and geometrical arrangement (and hence entropy), or by the strength of the attractive and rapidly decaying terms. For this latter kind of systems they argue that most of the behaviours encountered in hard-sphere dominated fluids will not be met. In this respect, the lack of a quantitatively accurate estimate of the freezing line of C_{60} when the entropic or the Hansen–Verlet prescriptions are adopted, could be interpreted rather than as a 'failure' of the criteria themselves, as a manifestation of their only qualitative applicability in this context.

3. Onset of crystallization in the metastable phase of a generalized Lennard-Jones model of globular protein solutions

We have investigated by MD simulations [17] the phase transformations occurring in a system of spherical particles interacting through the short-range potential

$$V(r) = \frac{4\epsilon}{\alpha^2}\left\{\left[\left(\frac{r}{d}\right)^2 - 1\right]^{-6} - \alpha\left[\left(\frac{r}{d}\right)^2 - 1\right]^{-3}\right\} \tag{4}$$

where d is the distance of minimum approach between two particles. The potential (4), shown in figure 1, constitutes a generalization of the Lennard-Jones potential; the parameter α determines the range of the attractive interactions with respect to the range d of the repulsive part; in particular, large values of α correspond to a deep and narrow attractive well. The model (4), with $\alpha = 50$, has been recently adopted by ten Wolde and Frenkel to study the phase behaviour of globular protein solutions [16]. The phase diagram of such a fluid is characterized by the absence of a stable liquid phase [16]; this is shown in figure 6, where it appears that the binodal critical point lies beneath the sublimation line, thus making liquid–vapour metastable with respect to solid–vapour equilibrium.

In a previous study of the aforementioned fluid [17], the investigation has been focused on the crystallization process, which represents the necessary and often limiting step in the experimental determination of protein structures. In particular, extensive MD simulations were performed in the NVE ensemble, along the isochore path at $\rho\sigma^3 = 0.5$, by starting from a well equilibrated sample in the homogeneous fluid region at $T/\epsilon = 1$ (see figure 6) and by inducing metastability by progressively cooling the system below the fluid–solid and the (metastable) liquid–vapour coexistence. All simulations concerned a sample of 2592 particles, enclosed in a tetragonal box with periodic boundary conditions and with box sides such that $L_x = L_y$ and $L_z = 3L_x$; with such a choice, the phase separation occurs by forming an interface perpendicular to the z-axis, which corresponds to the lowest interfacial area.

The important property of this model is that, down to large undercoolings, crystallization does not occur by a catastrophic process, as often observed with Lennard-Jones potentials, suggestive of mechanical instabilities in the system. Instead, it takes place by a sequence of events that are reminiscent of classical nucleation theory, extending on a time scale that is suitable for a detailed analysis by MD simulation. Moreover, the initial nucleation events appear to be well localized in space, reducing the effect of the small size of the simulation cell.

These properties allow one to analyse in detail how the crystallization process occurs in a simulated system, and to study the interplay of crystallization with the metastable liquid–vapour separation. The simulation runs were extended over very long trajectories (up to 76×10^6 MD steps), corresponding to a real time span of the order of μs, if the parameters of the potential are interpreted in terms of typical globular protein sizes, masses and interaction strengths.

Within the time span of the simulation, no phase transition was observed above the metastable binodal line, despite the high degree of undercooling for the homogeneous fluid phase. The absence of nucleation is probably due to the high surface tension of the crystal–fluid interface. Upon crossing the liquid–vapour line, one can observe the corresponding phase separation that occurs with only limited hysteresis. The liquid–vapour state appeared to be stable during simulations of ordinary length (i.e. of the order of 10^6 MD steps, or 10^3 characteristic time units) down to $T = 0.37$, a temperature $\sim$8% below the fluid–fluid phase separation line. At this temperature, crystallization started with only a negligible thermal activation.

A sequence of snapshots of MD configurations at progressively decreasing temperatures is shown in figure 7, together with the radial distribution functions for each temperature. The shapes of the radial distribution functions, with the rapid heralding of structured peaks in the tiny temperature range between 0.41 and 0.38, document quantitatively the sequence of phase transformations.

The adopted modelization of globular protein solutions is by all means a drastic one. Nonetheless, qualitative similarities survive in agreement with experimental data. We observe, for instance, that the metastable liquid–vapour separation dramatically enhances the crystallization kinetics, very likely because the presence of a high density fluid decreases both the interfacial free energy requested to nucleate the crystal, and the amplitude of the density fluctuation required to reach the solid density. We also observe that crystallization appears not to be accompanied by any precursor effect; in fact, when any of the criteria we devised to this aim were met, the nucleation process was in any case already well underway. Our observations do not strictly prove, however, that precursors do not exist, but only that the chain of events leading to the transition involves the non-trivial coupling of several variables, as shown experimentally in [26]. We refer the interested reader to the original papers [17] for more details.

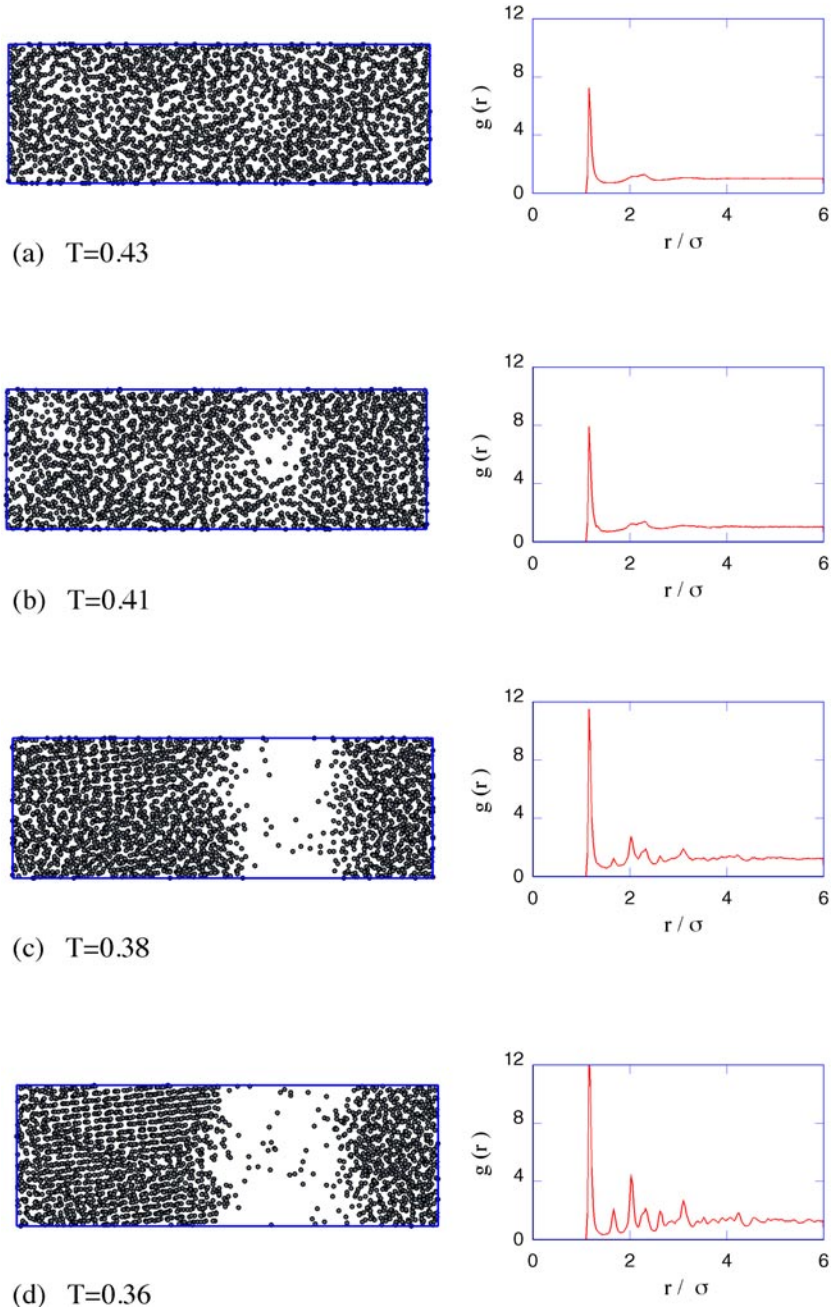

Figure 7. Snapshots of MD configurations at progressively decreasing temperatures together with the corresponding radial distribution functions; (*a*) $T = 0.43$, metastable homogeneous fluid; (*b*) $T = 0.41$, low-density bubble in a high-density fluid, just below the metastable liquid–vapour separation; (*c*) $T = 0.38$, crystal nucleus in the high-density fluid; (*d*) $T = 0.36$, extended defective crystal phase.

(This figure is in colour only in the electronic version)

4. Conclusions

The reported results concern the phase behaviour of two different model potentials characterized by a rapid decay of the interaction strength with the distance. As is apparent from figure 1, the first potential considered, initially proposed by Girifalco to model C_{60}, substantially vanishes within twice the zero potential distance. The phase diagram of such a model exhibits, according to the free energy calculations that we have reported here, a well defined, albeit narrow (in temperature), liquid pocket. This result further assesses similar previous estimates by various authors, and substantially confirms the first evidence of the existence of the liquid phase for such a model C_{60} [7]. We discuss the emerging discrepancy with the triple point temperature estimates based on one-phase freezing criteria [7, 11, 15].

It is also worth noting the deep transformation undergone by the phase diagram of short-range potential models, induced by tiny variations in the long-range decay of the interaction forces. This emerges from the comparison of the Girifalco with the generalized Lennard-Jones potential (see figure 1). We observe that the differences between the two patterns are rather small; yet, they are sufficient to induce profound modifications in the phase diagram and phase behaviour of the two models. In fact, the stable liquid phase disappears for the shorter-range potential, the liquid–vapour line shifting considerably beneath the sublimation line. The peculiar nature of such a metastable binodal curve emerges from MD simulations, which show that only when liquid–vapour separation takes place, does the crystallization process really start in the metastable fluid phase.

Acknowledgment

We wish to thank Professor P V Giaquinta for a useful discussion.

References

[1] George A and Wilson W 1994 *Acta Crystallogr.* D **50** 361
Rosenbaum D F, Zamora P C and Zukoski C F 1996 *Phys. Rev. Lett.* **76** 150
Lomakin A, Asherie N and Benedek G B 1996 *J. Chem. Phys.* **104** 1646
Malfois M, Bonneté F, Belloni L and Tardieu A 1996 *J. Chem. Phys.* **105** 3290
Piazza R, Peyre V and Degiorgio V 1998 *Phys. Rev.* E **58** 2733
Rosenbaum D F, Kulkarni A, Ramakrishnan S and Zukoski C F 1999 *J. Chem. Phys.* **111** 9882
[2] Louis A A, Allahyarov E, Löwen H and Roth R 2001 *Preprint* cond-mat/0110385 and references therein
[3] Girifalco L F 1992 *J. Phys. Chem.* **96** 858
[4] Pacheco J M and Prates-Ramalho J P 1997 *Phys. Rev. Lett.* **79** 3873
[5] Verheijen M A *et al* 1992 *Chem. Phys.* **166** 287
Kniaz K, Girifalco L A and Fischer J E 1995 *J. Phys. Chem.* **99** 18 804
Abramo M C and Caccamo C 1996 *J. Phys.: Condens. Matter* **57** 1751
Zubov V I 2000 *Mol. Mater.* **13** 385
[6] Schwarz U S and Safran S A 2000 *Phys. Rev.* E **62** 6957 and references therein
[7] Cheng A, Klein M L and Caccamo C 1993 *Phys. Rev. Lett.* **71** 1200
[8] See e.g. Muschol M and Rosenberger F 1997 *J. Chem. Phys.* **107** 1953
[9] McPherson A 1982 *Preparation and Analysis of Protein Crystals* (Krieger)
[10] Hagen M H J, Meijer E J, Mooij G C A M, Frenkel D and Lekkerkerker H N W 1993 *Nature* **365** 425
[11] Caccamo C, Costa D and Fucile A 1997 *J. Chem. Phys.* **106** 255
[12] Hasegawa M and Ohno K 1999 *J. Chem. Phys.* **111** 5955
Hasegawa M and Ohno K 2000 *J. Chem. Phys.* **113** 4313
[13] Giaquinta P V and Giunta G 1992 *Physica* A **187** 145
[14] Hansen J-P and Verlet L 1969 *Phys. Rev.* **184** 151
[15] Caccamo C 1995 *Phys. Rev.* B **51** 3387
[16] ten Wolde P R and Frenkel D 1997 *Science* **277** 1975
[17] Costa D, Ballone P and Caccamo C 1999 *(AIP Conf. Proc. vol 513)* ed A Messina (New York: Melville)

Costa D, Ballone P and Caccamo C 2001 *J. Chem. Phys.* (accepted)
[18] Hansen J-P and McDonald I R 1986 *Theory of Simple Liquids* 2nd edn (London: Academic)
[19] Frenkel D and Ladd A J C 1984 *J. Chem. Phys.* **81** 3188
[20] Frenkel D and Smit B 1996 *Understanding Molecular Simulation* (London: Academic)
[21] Widom B 1963 *J. Chem. Phys.* **39** 2808
[22] Abramo M C, Caccamo C, Costa D and Pellicane G 2001 *Europhys. Lett.* **54** 468
[23] Caccamo C 1996 *Phys. Rep.* **274** 1
[24] Saija F, Prestipino S and Giaquinta P V 2001 *J. Chem. Phys.* **115** 7586
[25] Louis A A 2001 *Phil. Trans. R. Soc.* A **359** 939
[26] Schätzel K and Ackerson B J 1992 *Phys. Rev. Lett.* **68** 337